JOURNAL OF MATERIALS SCIENCE 8 (1973) 1201–1212

Review
Associated point defects in II-VI compounds

R. K. WATTS
Physical Sciences Research Laboratory, Texas Instruments Incorporated, Dallas, Texas, USA

Recently, the structures of many associates of point defects in the II-VI compounds have been determined. The status of present knowledge is reviewed with emphasis on the arguments leading to models for the various associates.

1. Introduction

In the last several years the microscopic structures of many defects in crystalline solids have been elucidated by optical, magnetic resonance, electrical, and chemical experiments. The defect state of solids has proved to be quite complex. As well as isolated native defects and isolated dopant atoms, associates of these defects often occur forming what can usefully be considered small molecules embedded in the crystal. The formation of associates can drastically affect the electrical and optical properties of crystals. Improved understanding of association phenomena should lead to greater ease in tailoring materials for desired properties.

This paper reviews the experimental results obtained for associated point defects in the II-VI compounds, the chalcogenides of zinc and cadmium. The mercury compounds are excluded. CdO will also be excluded because of its different crystal structure. The compounds of interest normally have either the sphalerite or wurtzite crystal structure. Both are four-co-ordinated structures. In the cubic sphalerite structure shown in Fig. 1 the neighbours of a cation site are a first shell of four anions along ⟨1 1 1⟩ directions, a second shell of twelve cations along ⟨1 1 0⟩ axes, a third shell of twelve anions along ⟨3 1 1⟩ directions, etc. The wurtzite structure is somewhat similar but has hexagonal symmetry. A large number of associate types has been discovered in these compounds, perhaps largely because they have certain properties which have made the experiments more fruitful.

An associate will be defined as a close grouping of two or more simple defects, where a simple defect is taken to be an atom of the host crystal not on its normal site, a vacancy, or a foreign atom. Thus donor-acceptor pairs separated by many lattice spacings [1] are not considered. Electrons or holes trapped by cations or anions of the host lattice will not be considered simple defects; this restriction excludes, for example, the centre in ZnO consisting of a substitutional lithium and a hole trapped on a nearest-neighbour oxygen [2].

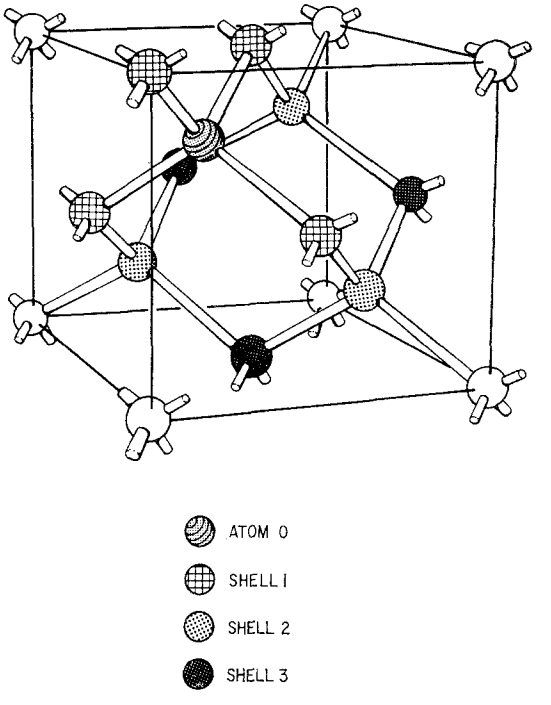

Figure 1 Near neighbours of a site in a lattice of sphalerite structure. The first shell of neighbours of a cation contains four anions at distance d along the ⟨1 1 1⟩ axes. The second shell consists of twelve cations at distance $1.632d$ along the ⟨1 1 0⟩ axes. The third shell consists of twelve anions at distance $1.918d$ along ⟨3 1 1⟩ axes.

In the next section, a brief outline of the chemical theory of association of defects is given. The third section discusses the most useful experimental techniques. The fourth part reviews the experimental results and also contains a few new, previously unpublished, observations. Some of the associates will seem to have rather surprising, unexpected structures. In order that the review be of interest to the general reader, much of the detailed data will not be included, but only enough to show how the structures of the associates are deduced.

2. Chemical theory of association

Suppose two simple defects A and B form an associate AB with an enthalpy change ΔH according to the reaction

$$A + B \rightleftharpoons AB + \Delta H .$$

If the simple defects and the associates are assumed to be randomly distributed, the concentrations are related by the mass action law

$$[AB][A]^{-1}[B]^{-1} = \exp(-\Delta G/kT) , \qquad (1)$$

where $\Delta G = \Delta H - T\Delta S$ is the corresponding change in Gibbs free energy. The entropy change, ΔS, depends largely upon the number of equivalent arrangements possible for the associate, and the enthalpy change ΔH is due to the interaction between A and B-electrostatic, covalent bonding, short range repulsion, etc [3]. For the case of oppositely charged defects interacting only by Coulomb attraction the distribution of B defects about an A defect as a function of distance from A has been found by several workers. In one derivation, use is made of the mass action law and the crystal is treated as a continuum [4], while another is based on more fundamental probabilistic considerations, and the discrete nature of the crystal lattice is taken into account [5]. The results of both treatments are very similar, however. The distribution has two peaks, one near the distance of closest approach and another near the separation expected for a completely random distribution. These peaks are separated by a minimum at the distance where the interaction energy is equal to the thermal energy $2kT$. If the binding energy is greater than $2kT$, then, there is a tendency toward association. The actual situation in a polar solid is more complex, involving polarization, rearrangement of nearby atoms, and covalent effects, but the simple model gives a good qualitative description of association.

If A and B are two oppositely charged impurity ions of equal total concentration interacting only by Coulomb attraction, Equation 1 can be used to calculate the fraction paired at each of the possible separations (nearest neighbour, third nearest neighbour, etc)

$$\Delta H = -q^2/\epsilon r , \qquad (2)$$

where q and $-q$ are the charges of the two ions with separation r. The interaction is screened by the dielectric constant ϵ of the material. Often only the two or three smallest separations need be considered, since almost the whole contribution to pairing comes from these [6]. For example, the fraction paired at separation r_j will be much larger than the fraction paired at the larger separation r_k if

$$(q^2/\epsilon kT)(r_j^{-1} - r_k^{-1}) \gg 1 . \qquad (3)$$

The fraction paired depends strongly on the total concentration [A] + [AB] and on the temperature. At low concentration a large fraction can be paired only at low temperatures. As concentration increases, appreciable pairing can occur at higher temperatures. Of course, pairing at low temperatures may occur so slowly, because the defects may have very low mobility, that it would not be observable. Interstitial atoms can be mobile at very low temperatures [7], however, and associates involving interstitials should form more readily. The time development of the approach to an equilibrium situation in pairing has been treated by Reiss *et al* [4]. Electrically neutral defects may also form associates; they may exchange an electron to become charged and then interact electrostatically [3].

Even a crystal free from impurity atoms will always contain a number of native defects at non-zero temperature, since the creation of a vacancy, for example, requires only a finite amount of energy. A substitutional impurity is incorporated by interaction with a vacancy. The vacancy concentration affects the solubility of the impurity. Diffusion of impurities usually also requires the presence of vacancies.

Donor or acceptor impurities introduced into II-VI compounds are always largely compensated by native defects. This self-compensation has been explained in the following way [8]. Energy must be supplied by the crystal to produce the compensating native defects, while energy is gained by the interaction of the native defects with the free carriers produced by the

dopant. The energy gained upon recombination of a free carrier at a vacancy is roughly equal to the bandgap, while the energy necessary for creation of a vacancy correlates with the cohesive energy. Since the ratio of bandgap to cohesive energy is near one for these compounds, considerable self-compensation is to be expected. Associates of impurities and native defects might be expected to occur. Indeed these have been observed as well as impurity-impurity associates.

Results of the experimental studies reviewed here have rarely been related to the chemical theory of association. The experiments have been directed toward structure determination. The theory is mentioned here because it can predict that most associates will occur with the smallest possible separation between components. This has been found to be the actual situation.

3. Experimental methods

Structural information for associate centres has largely come from magnetic resonance and optical experiments with supporting evidence occasionally obtained from chemical and electrical measurements. Most associates have a lower symmetry than that of the host lattice, and often experiments are designed to reveal this lower symmetry as an indication of association. Very detailed information often results when the associate is characterized by a well localized wavefunction.

Optical absorption or luminescence due to a transition between energy levels of a localized defect centre may show polarization other than that ascribable to overall crystal symmetry. Suppose for example that a certain defect centre in a crystal of sphalerite structure has ⟨111⟩ axial symmetry. There will be four types of centre corresponding to the four ⟨111⟩ directions. Suppose also that the defect centre has an absorption band and, at longer wavelength, an emission band, both associated with transitions between localized energy levels of the defect. In general the intensity of emitted light and the absorption strength will be different depending whether the polarization vector is parallel or perpendicular to the axis of the defect centre. Thus absorption of light polarized parallel to a ⟨111⟩ axis (and, therefore, making an angle of 70.5° with the other three ⟨111⟩ directions) may lead to partially polarized emission, implying a lower symmetry for the defect than that of the host lattice. The II-VI compounds have either the sphalerite or wurtzite crystal structure [9]. CdS and ZnO always have the wurtzite structure; ZnTe and CdTe always have sphalerite structure. The hexagonal wurtzite structure will in general produce polarization effects. Many ZnS and ZnSe crystals of sphalerite structure contain stacking faults parallel to one of the {111} planes, and these can cause polarization also. Koda and Shionoya [10] were able, for example, to measure polarization of the "self-activated" blue luminescence in ZnS and to ascribe the polarization to oscillating electric dipoles oriented along the ⟨111⟩ directions. When the absorption or luminescence line is narrow enough, the symmetry of the defect can be found from the angular dependence of the Zeeman effect [11]. In principle, symmetry information can also be extracted from Raman scattering by electronic or localized vibrational excitations, but large concentrations are usually necessary for adequate signal strength.

Electron paramagnetic resonance or EPR is a powerful tool for investigation of associates. Of course the defect must have an unpaired electronic spin. By illuminating the crystal at low temperature with light of bandgap energy one can often cause a defect to become paramagnetic by trapping a hole or electron. The unpaired spin of angular momentum, $(h/2\pi)\boldsymbol{S}$, has associated with it a magnetic moment $\beta \boldsymbol{g} \cdot \boldsymbol{S}$, where β is the Bohr magneton. The tensor, $\boldsymbol{g}$, has the symmetry of the defect. $\boldsymbol{S}$ is the electronic spin (or a combination of this with an orbital contribution). By observing the resonance while varying the direction of the static magnetic field with respect to the crystallographic axes, one determines the symmetry and principal values (g factors) of $\boldsymbol{g}$. Fig. 2 shows the angular dependence of resonances due to four centres of ⟨111⟩ axial symmetry, obtained by rotating the magnetic field in a {110} plane. One can immediately see from such a plot that the centre has ⟨111⟩ axial symmetry. The magnitudes of the g factors contain information about the ground state wave function of the defect.

Some orbitally degenerate states are very sensitive to strains along certain crystallographic directions [12]. These Jahn-Teller active states by interacting with lattice strains can cause a lowering of the symmetry of the defect in these states. This effect must be separated in analysis from lowering of the symmetry caused by association. One way of accomplishing this is by application of a uniaxial stress at a low enough temperature that defects are not mobile; the

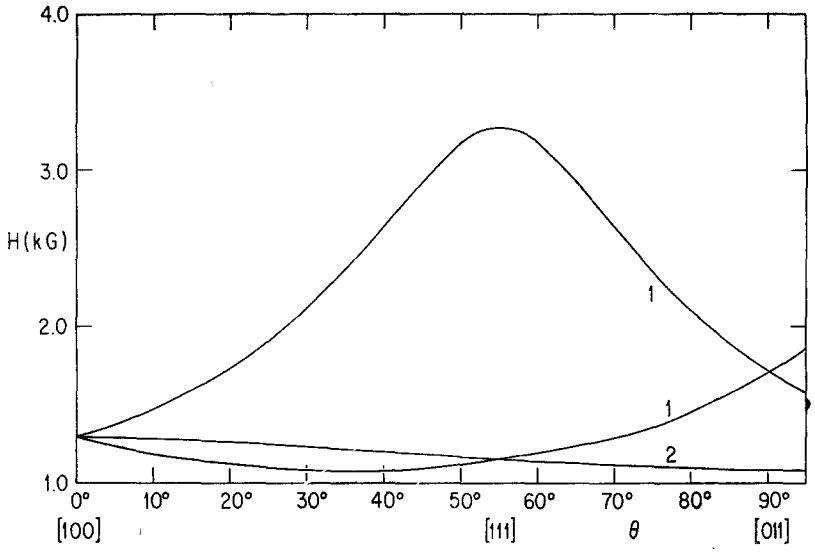

Figure 2 Angular dependence of the resonance field for four ⟨111⟩ centres with $g_{\parallel} = 2$, $g_{\perp} = 6$ and a 9.2 GHz resonance frequency. The magnetic field is parallel to the (011) plane. θ is the angle between the field and [100]. One curve represents resonance from twice as many centres as either of the other two.

stress may cause a reorientation of some of the centres implying that the low symmetry is not due to association. The reorientation is apparent through a redistribution of intensities in the spectra. For example the spectrum due to centres with symmetry axis parallel to the direction of applied stress may increase (or decrease) in intensity relative to the spectra of centres with other symmetry axes.

The unpaired electronic spin interacts with the nuclear magnetic moments of the nuclei in its vicinity. This hyperfine interaction leads to a splitting of the resonance line or to a broadening, depending upon the strength of the interaction. The host lattice constituents of the II-VI compounds have isotopes of non-zero nuclear spin only in low abundance, see Table I. This leads to narrow lines in the EPR spectra and a concomitant precision and wealth in the information available therefrom. The III-V compounds on the other hand are composed of nuclei all of which have nuclear spins; EPR has consequently been of little use in studying defects in these materials.

TABLE I Isotopes of non-zero nuclear spin in II-VI lattices.

Isotope	Nuclear spin I	Abundance (%)
Zn^{67}	5/2	4.1
Cd^{111}	1/2	12.8
Cd^{113}	1/2	12.3
O^{17}	5/2	0.037
S^{33}	3/2	0.75
Se^{77}	1/2	7.5
Te^{123}	1/2	0.88
Te^{125}	1/2	7.0

Interaction with a nuclear spin I causes a splitting into $2I + 1$ lines. The hyperfine splittings and their angular dependence can show which atoms are present at the defect and where they are located. These effects can be enhanced or deductions made from them confirmed by the use of dopants artificially enriched with isotopes of particular nuclear spin [13]. Interaction with the host nuclei shown in Table I is often observable also. When hyperfine interactions are so small as to lead only to a broadening of the line, they can sometimes still be studied in detail by means of an electron-nuclear double resonance technique (ENDOR) [14].

There are several ways to identify a defect observed by EPR as the same defect seen optically or electrically. In practice it is often difficult to eliminate ambiguity from such a correlation, however. Perhaps the wavelength of light which enhances or quenches the EPR signal also produces photoconductivity or luminescence. When the defect contains a rare earth impurity, the optical Zeeman effect may be used to make an unambiguous identification,

since rare earth optical spectra contain narrow lines. The g factors of ground and excited state are obtained. If the ground state g factor is the same as that measured by EPR, the correlation is made.

4. Observed associates

The first few associates described below contain iron. Iron is a well-known "killer" of luminescence in the II-VI compounds. All of the atoms with which iron has been shown to form associates give rise to characteristic luminescences in the absence of iron. Most of the resonances due to iron associates are not photosensitive. Iron kills luminescence by associating with the luminescence activator; the associate has a very different system of energy levels and is not an activator.

4.1. Fe-As

This associate has a very simple structure. A cation is replaced by an Fe^{3+} iron and one of the four nearest anions by an As^{3-}. The defect has been observed in ZnSe by EPR [13]. The resonance is seen at liquid helium temperatures in crystals doped with arsenic. Iron is a common contaminant in all II-VI compounds. Intentional doping with iron causes the signal to increase.

The g tenor is axially symmetric, the symmetry axis being a $\langle 1\,1\,1\rangle$ direction. For a general orientation of the magnetic field four resonances are seen corresponding to defects with each $\langle 1\,1\,1\rangle$ symmetry axis. See Fig. 2. Thus with the magnetic field parallel to [1 1 1] two resonances are observed: one from defects whose symmetry axis is [1 1 1], which occurs at the magnetic field value

$$H(0°) = h\nu/\beta g_{\parallel},$$

where ν is the resonance frequency, and another from defects whose symmetry axes are the other $\langle 1\,1\,1\rangle$ directions, all at 70.5° from the field direction and occurring at the field

$$H(70.5°) = h\nu/[\beta(g_{\parallel}^2 \cos^2 70.5° + g^2{}_{\perp} \sin^2 70.5°)^{\frac{1}{2}}].$$

$g_{\parallel}$ and $g_{\perp}$ are the principal values of g, and the subscripts refer to the $\langle 1\,1\,1\rangle$ symmetry axis. The parallel spectrum at $H(0°)$ is shown in Fig. 3. The four strong lines are due to a hyperfine interaction with one As^{75} nucleus (abundance 100%). The five weaker lines come from interaction with three Se^{77} nuclei (abundance 7.5%),

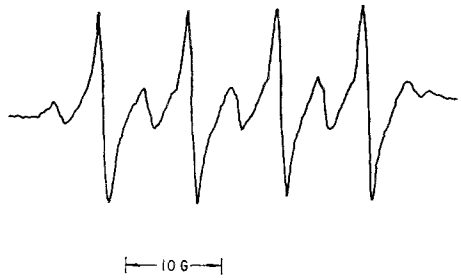

Figure 3 Resonance spectrum from Fe-As associates whose $\langle 1\,1\,1\rangle$ symmetry axis is parallel to the magnetic field. The four strong lines are due to hyperfine splitting from interaction with the As nuclear moment, and the five weaker lines are due to interaction with three equivalent Se nuclei.

which are equivalently located with respect to the magnetic field.

The ground electronic configuration of Fe^{3+} is $(3d)^5$. In a trigonal electric field the $^6S_{5/2}$ state splits into three doublets. The doublet $M_S = \pm \frac{1}{2}$ should have g factors $g_{\parallel} = 2$, $g_{\perp} = 6$, as observed. In a sample doped with iron isotopically enriched to 98% Fe^{57} with nuclear spin $I = \frac{1}{2}$ the spectrum of Fig. 3 is doubled, as shown in Fig. 4. The natural abundance of Fe^{57} is 2.2%, the rest having zero nuclear spin.

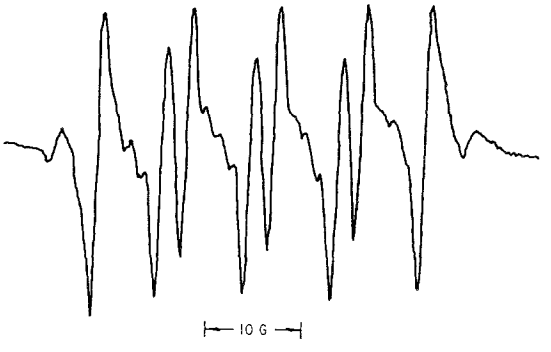

Figure 4 Resonance spectrum from Fe^{57}-As associates whose $\langle 1\,1\,1\rangle$ symmetry axis is parallel to the magnetic field. The doubling of the spectrum of Fig. 3 is due to a hyperfine interaction with the Fe^{57} nuclear moment.

From the observations the following conclusions can be drawn. The paramagnetism is located largely on the iron. The trigonal electric field is rather large, splitting the $M_S = \pm 3/2$ and $M_S = \pm 5/2$ doublets away from the lowest $M_S = \pm \frac{1}{2}$ doublet by an energy much larger than the microwave quantum (0.35 cm^{-1}). This large electric field is produced by a single arsenic ion replacing one of the four nearest neighbour

seleniums. The probable charge state of the arsenic is -3, providing charge compensation for the iron. By means of the hyperfine splittings, the four nearest neighbours of the iron could be observed directly.

The iron and arsenic impurities were added to the melt. The crystals were grown by a special method at greater than atmospheric pressure because of the volatility of arsenic [15]. The associate occurs because its binding energy is large compared with thermal energy at the temperature at which it forms.

4.2. Fe-Se and Fe-2Se

The resonance spectra of these associates have been observed by Schneider *et al* [16] in mixed $ZnS_{1-x}Se_x$ crystals with x small. The Fe-Se centre consists of Fe^{3+} on a zinc site with one neighbouring sulphur replaced by a selenium and is similar to the Fe-As associate. The spectrum shows $\langle 111 \rangle$ axial symmetry and hyperfine interactions from Fe^{57} and Se^{77} nuclei. In the Fe-2Se associate two of the four nearest sulphurs are replaced by selenium. The spectrum has orthorhombic symmetry corresponding to the C_{2v} symmetry of the FeS_2Se_2 cluster. The rather large splitting of the Fe^{3+} $^6S_{5/2}$ state in this case probably is due to a difference in the covalent contributions to the Fe-Se and Fe-S interactions. Similar associates containing manganese instead of iron were also observed.

4.3. Fe-6F

Kravitz and Piper [14] have identified an associate of iron with six fluorines in CdTe. The resonance spectrum of Fe^{3+} with strong hyperfine interactions with six fluorines was studied both with EPR and ENDOR. The cluster is an $(FeF_6)^{3-}$ molecule ion with the fluorines along the six $\pm\langle 100 \rangle$ directions. The complex does not bond appreciably with the host lattice and it is not known at what site the cluster is incorporated.

4.4. Fe-Cu, Fe-Ag, and Fe-Li

Magnetic resonance spectra of associates of iron with copper, silver, or lithium have been observed by several workers in many of the II-VI compounds. The most definitive investigation is that of Holton *et al* [17]. They observed the Fe-Cu associate in ZnS, ZnSe, ZnTe, and CdTe, the Fe-Ag associate in ZnS, and the Fe-Li associate in ZnS and ZnO. Similar associates have been reported by Kemp in CdS containing iron and copper [18] or iron and lithium [19] and by Morigaki and Hoshina [20] in CdS intentionally doped only with iron. For Fe-Cu in ZnS, ZnSe, and ZnTe the defect with which the iron associates could be identified by hyperfine structure, but in the other cases this was not possible.

In crystals with the cubic sphalerite structure very anisotropic EPR spectra characteristic of Fe^{3+} in an electric field of C_s symmetry are observed. Resonances from both the lowest and next lowest doublet were seen. Analysis of the complex angular dependence of the spectra shows that they arise from twelve crystallographically equivalent iron defects. The orientation of the principal axes of the g tensor of one of these is shown in Fig. 5. In the case of Fe-Cu the Cu^{63}

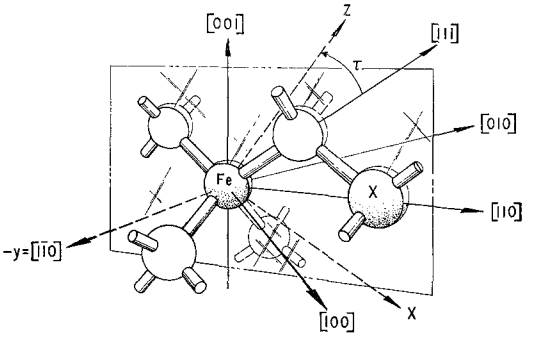

Figure 5 Model of the Fe-X centres. X represents Cu, Ag, or Li. The principal axes of the g tensor (x, y, z) are shown. The angle τ varies with X and with host crystal.

and Cu^{65} hyperfine splittings are seen and prove that one copper ion is associated with the iron in each associate. It seems likely that both iron and copper would occupy cation sites. A Cu^+ ion on a nearby cation site provides charge compensation and would be diamagnetic, as observed. Considering the first fifteen cation shells around a central cation site, Holton *et al* find that only by occupying the sites of the first, fourth, or fifteenth shell could copper form twelve associates of C_s symmetry. The magnitude of the copper hyperfine interaction is that expected for an ion in the first cation shell. If some shell other than the first were occupied by the copper, one might expect to see the first shell associates as well; these are not observed. Furthermore Cu^+ at a nearest Zn site can produce the kind of electric field responsible for the orthorhombic g. Association models involving interstitials are in poor agreement with the results. The associate,

then, has the structure shown in Fig. 5. Fe-Ag and Fe-Li dopings each produce twelve spectra very similar to those of Fe-Cu. The same type of associate is probably formed in these cases also.

In the wurtzite lattices the twelve nearest cation sites corresponding to the first cation shell of the sphalerite structure are not all crystallographically equivalent. Consequently there can be three different types of associate formed on these and the central cation site. All three types form in ZnO [17].

4.5. SA associates

When ZnS or ZnSe is doped with chlorine, bromine, iodine, aluminium, or gallium, an associate of the impurity with a zinc vacancy is formed. This SA defect is responsible for the well-known "self activated" luminescence. The singly negative group VII ion replaces one of the four anions nearest the vacancy, or the tripositive group III ion substitutes for a nearest zinc. Such an associate has one excess negative charge with respect to the lattice and can compensate an ionized shallow donor – isolated substitutional Cl^- or Al^{3-}, for example. In this manner, the donors are self compensated and do not make the crystal n type conducting. When the SA defect traps a hole it becomes paramagnetic. The structure of the SA centre has been determined during the last several years by optical and magnetic resonance experiments.

The optical properties of all the SA centres are quite similar [21]. The luminescence band is broad and of Gaussian shape. The emission occurs in the blue in ZnS and in the red in ZnSe, the peak for the group VII centres occurring at slightly higher energy than for group III centres. The excitation spectrum of this luminescence has two peaks, one at bandgap energy and another at lower energy. The luminescence shifts to lower energies with decreasing temperature, opposite to the shift of the bandgap. The functional forms of the dependence on temperature of the luminescence peak position and width are in good agreement with the predictions of the configuration co-ordinate model [10]. These observations imply that the luminescence occurs by a transition between well-localized states of a defect.

Koda and Shionoya [10] found that the self activated luminescence in cubic ZnS is polarized under polarized excitation and that the polarized emission from the defect in its diamagnetic charge state [22] is due to σ electric dipole oscillators oriented along the four $\langle 1\,1\,1\rangle$ directions. From this they inferred that the chlorine is associated with another simple defect along the $\langle 1\,1\,1\rangle$ axis.

The EPR spectra of the paramagnetic charge state of the SA centre, produced by irradiation of the sample with ultra-violet light, have been investigated by several people [21, 23-25]. At liquid helium temperatures all of the spectra display monoclinic symmetry with a $\{1\,1\,0\}$ mirror plane, and the hole is trapped on one sulphur or selenium, as shown by observation of a hyperfine interaction with a single S^{33} nucleus [21]. The presence of the group VII or group III impurity in the defect has also been established from hyperfine splittings [26, 27]. In the case of the group III SA centres it is obvious how the low C_S symmetry of the defect arises. Of the four sulphurs around the vacancy the hole prefers the one furthest from the Al^{3+}. See Fig. 6. For

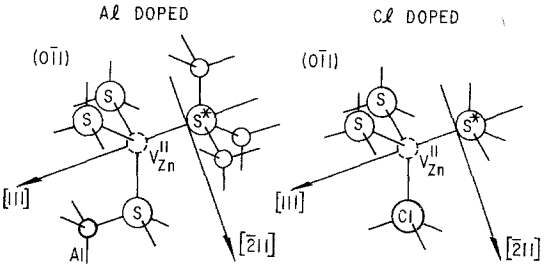

Figure 6 Models of the two types of SA centre in ZnS. The asterisk indicates a trapped hole.

the group VII SA centres the three sulphurs are equivalent, however. But because of the degeneracy associated with the three sulphur sites a spontaneous Jahn-Teller type distortion of the complex occurs lowering the symmetry from C_{3v} to C_s. Because of the distortion, localization of the hole on a single sulphur is now energetically more favourable. As the temperature is raised, the hole hops among the three equivalent distortions. When this hopping becomes rapid enough, the lower symmetry is averaged out and the axial C_{3v} symmetry is observed [28]. The SA centre has also been seen in hexagonal ZnS. Schneider *et al* [27] have studied the SA centre in mixed $ZnS_{1-x}Se_x$ crystals. They find that when one of the sulphurs in the complex is replaced by a selenium, the hole is localized on the selenium. When two sulphurs are replaced by selenium, the hole is found in a molecular orbital localized on the two seleniums. This is to be expected, since the valence electrons of selenium are less tightly bound than those of sulphur.

The photosensitivity of the EPR spectra has made it possible to show that the same defect is responsible for the optical and magnetic properties. As the temperature of the crystal is raised from a low value, thermoluminescence occurs accompanied by a decrease in the EPR signal. Illumination with 1.4 eV light quenches the EPR signal and the SA thermoluminescence [28]. Also, illuminating the crystal at low temperature with polarized light of wavelength corresponding to the lower energy excitation band creates preferentially EPR spectra of SA centres of one orientation, dependent upon the direction of polarization [29].

The presence of the vacancy in the associate is difficult to prove, but it is indicated by several pieces of evidence. The optical polarization measurements show that the halogen is associated with another defect along the ⟨1 1 1⟩ axis. More SA centres are formed when the number of available zinc vacancies is increased by higher partial pressure of sulphur during preparation [30]. Molecular orbital models and crystal field calculations, which assume a vacancy present, are able adequately to describe the experimental results [27, 28].

These optical and magnetic properties are described by the following model [10, 21]. The diamagnetic SA centre has an occupied ground state above the valence band edge and an empty excited state slightly above the conduction band edge. Luminescence is produced in two ways. Bandgap excitation produces free holes and electrons, and some of the holes may be trapped at SA centres, subsequently to recombine with free electrons, producing luminescence, or, excitation into the lower energy band excites the centre to the unrelaxed excited state. The lattice around the excited centre relaxes lowering the excited state below the bottom of the conduction band, and luminescence occurs with the return to the ground state. The positions of these energy levels with respect to the band edges have been established. When electrons are released from traps to recombine with holes on SA centres, thermoluminescence and quenching of the EPR signal result. The polarization effect on the EPR occurs when diamagnetic centres of different orientation are preferentially raised to the excited state from which ionization may occur before the state relaxes below the conduction band edge.

4.6. Rare earth associates

The rare earth ions have very characteristic optical spectra whose gross features are insensitive to the crystalline environment. Interpretation of the spectra is simplified by the absence of Jahn-Teller distortions. Thus whenever local symmetry lower than that of the unperturbed lattice site is seen in the optical or EPR spectra, association with another defect is indicated. The splittings of the ground multiplets of all the trivalent rare earth ions in tetrahedral crystal fields have been calculated by Lea *et al* [31]. They have also given wavefunctions for the sublevels of these multiplets. Watts and Holton [32] found that the observed g factor of a rare earth in the II-VI compounds is very nearly equal to that expected for one of the sublevels of the ground multiplet and that from an electrostatic point-charge model one can predict which sublevel lies lowest in energy. The associates discussed in the following four paragraphs were observed in crystals of sphalerite structure.

Crystals containing a rare earth and a noble metal (copper, silver, or gold) show three different types of rare earth EPR spectra: an isotropic resonance from unassociated substitutional rare earths, another isotropic resonance, and a resonance from the rare earth in a site with ⟨1 1 1⟩ axial symmetry. In CdTe the Yb^{3+} resonance of the second type shows [32] a hyperfine splitting from interaction with six equivalent tellurium nuclei along the ⟨1 0 0⟩ axes. The isotropic nature of the resonance implies that the ion is at a site of tetrahedral symmetry. Clearly the site is the interstitial site with six nearest telluriums along the ⟨1 0 0⟩ directions. The g factors are similar but quantitatively different depending whether the noble metal co-dopant is copper ($g = 2.525$), silver ($g = 2.511$), or gold ($g = 2.501$). This implies that the noble metal is near the Yb^{3+}. The linewidth of the Yb-Cu resonance is three times greater than in other cases, probably because of an unresolved hyperfine interaction with the large copper nuclear moment. The model of this associate is shown in Fig. 7. Four monovalent noble metal ions substitute for the four nearest cations. The g factors calculated from this model agree with the observed ones. The analogous $Er^{3+} - 4Ag^{+}$ and $Er^{3+} - 4Cu^{+}$ associates were observed by Kingsley and Aven [11] in ZnSe. They were able to correlate the optical and EPR spectra by means of the optical Zeeman effect.

In CdTe the axial Yb^{3+} resonance also shows a hyperfine interaction with six tellurium nuclei. The six are not equivalent, but are divided into

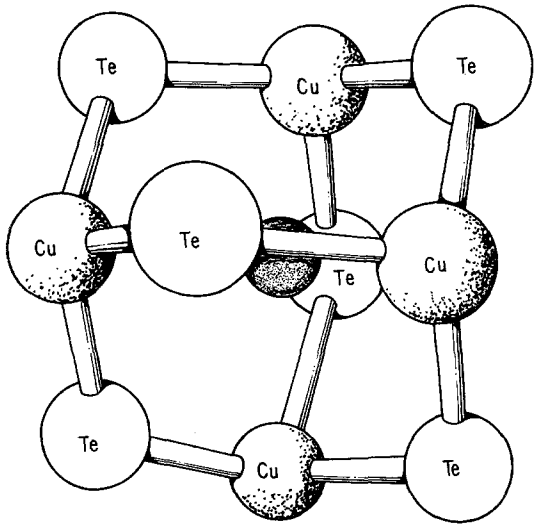

Figure 7 The Yb^{3+}-$4Cu^{+}$ centre. The small dark sphere represents the interstitial Yb^{3+}. Cu^{+} replaces the four nearest Cd^{2+} ions.

two groups of three equivalent atoms. Again the g factors are similar, but depend upon the noble metal dopant. The average g factors, $g_{\parallel}/3+2g_{\perp}/3$, are near the values for the $Yb^{3+}-4M^{+}$ defect. This resonance is due to Yb^{3+} in the same interstitial position, but with only three of the four nearest cadmiums replaced by Cu^{+}, Ag^{+}, or Au^{+}. A point-charge calculation based on this model predicts the observed average g factor and anisotropy, $g_{\parallel} > g_{\perp}$.

By similar arguments, Title and Mayo [33] have identified associates of interstitial Er^{3+} or Yb^{3+} with one substitutional Li^{+} in CdTe and of a substitutional Yb^{3+} or Er^{3+} with a P^{3-} substitutional for a nearest tellurium in ZnTe and CdTe. The phosphorus hyperfine interaction was observed in ZnTe.

Thulium-lithium associates have been observed by Masui [34] in ZnSe. The angular dependence of the optical Zeeman effect shows that the associate has axial symmetry about a ⟨100⟩ direction. The optical spectra were analysed and found to be compatible only with the following model. The Tm^{3+} ion is located at the second type of interstitial site whose near neighbours are four seleniums and six zincs. Four of the zincs in a {100} plane are replaced by Li^{+}.

4.7. Phosphorus cluster

An associate consisting of a cluster of four phosphorus atoms has been identified in ZnSe by Watts and Holton [35]. The EPR spectra are characterized by axial symmetry about the ⟨111⟩ directions, g factors near two, a large hyperfine interaction with one phosphorus nucleus, and smaller hyperfine interactions with three other equivalent phosphorus nuclei. The tensor characterizing the large hyperfine splitting has the same ⟨111⟩ axial symmetry as g, whereas that of the smaller interaction has ⟨110⟩ axial symmetry. The associate is a cluster of four phosphorus atoms located at the points of a regular tetrahedron. Two of the centres are shown in Fig. 8.

The paramagnetism is largely concentrated in a p orbital on one phosphorus, and the configuration is probably p^5. It is not possible to infer from the data how this complex is incorporated in the ZnSe lattice. Such tetrahedra occur about each substitutional and interstitial site. All of these sites could give rise to the observed hyperfine interaction with three equivalent seleniums when the magnetic field is parallel to the ⟨111⟩ symmetry axis. It seems most likely that phosphorus would substitute for the four zincs about one of the two interstices, one phosphorus having approximately the $(3s)^2(3p)^5$ configuration and the others, $(3s)^2$. Thus the complex has one excess negative charge. It is interesting to note that the P_4O_6, P_4O_{10}, and P_4S_{10} molecules have the same structure as the complex and its immediate neighbours would have at this site

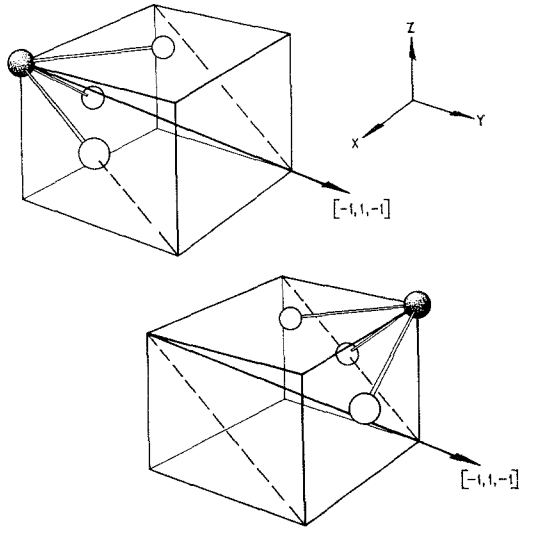

Figure 8 Orientation of two of the phosphorus clusters with respect to the ⟨100⟩ axes. The shaded ball represents the phosphorus on which the paramagnetism largely resides.

[36]. A compensating defect along the trigonal axis may make one phosphorus inequivalent to the other three.

4.8. Other copper associates

Copper is a well-known activator of luminescence in the II-VI compounds. Copper doping of ZnS under various conditions produces characteristic luminescence bands in the blue, green, red-orange, or infra-red. In addition to the Fe-Cu and rare earth-Cu associates already discussed, eleven different copper defects have been observed in II-VI compounds by EPR, eight of these in ZnS [37]. The copper is identified by its hyperfine structure. Seven of these defects were seen in crystals of sphalerite structure. All have axial symmetry about the $\langle 1\,1\,1\rangle$ direction, except one which has monoclinic symmetry. Although the $(3d)^9$ configuration of Cu^{2+} is subject to Jahn-Teller effects, it is clear that most of these defects must be associates.

Dieleman *et al* [38] have reported EPR measurements for a defect in red-orange luminescent ZnS doped with copper, silver, or gold. The three dopants produce similar spectra in powder samples. In the case of ZnS:Ag the angular dependence of the spectra were investigated in a single crystal. The spectra are characterized by g factors near two, $\langle 1\,1\,1\rangle$ axial symmetry, a small hyperfine interaction with one silver nucleus, and a very small hyperfine interaction with three equivalent zinc nuclei. The model proposed is the antimorph of the chlorine SA centre: a sulphur vacancy with one of the four nearest zincs replaced by Ag^+ (or Cu^+ or Au^+) and an electron localized on the other three. One would expect the electron density on the zincs to be comparable to that observed for the F centre in ZnS (a sulphur vacancy with an electron localized on the four nearest zincs). The zinc hyperfine splitting of the F centre is thirty times larger, however [39]. The photosensitive EPR signal was correlated with the optical spectra, and the defect has the same symmetry as Shionoya *et al* [40] found from measurements of polarized luminescence for the diamagnetic charge state of the copper red-orange defect. The author [37] found only the EPR spectrum of a different copper defect ("Cu-S") in the red-orange luminescent crystal of Shionoya *et al* and the spectrum of yet another copper centre ("Cu-H") in other crystals showing the same luminescence.

Urabe *et al* [41] have established that the blue copper luminescence is also due to a well localized defect with C_{3v} symmetry. Bowers and Melamed [22] showed that in the unexcited phosphor this defect, like the SA centre and the red-orange copper defect, is diamagnetic. An associate of an interstitial Cu^+ with a Cu^+ substitutional for a zinc has been proposed as a model for this centre, but must be regarded as speculative.

4.9. Manganese pairs

In all of the cases of association discussed above, except the Fe-Se associates, the concentrations of the simple defects from which the associates are formed were small. In most cases the simple defects had opposite effective charges, and it can be assumed that electrostatic attraction leads to association according to the theory outlined in Section 2. The Mn^{2+} pairs observed in ZnS are different. Sphalerite ZnS and βMnS have the same structure. Mn^{2+} pairs have been studied at high manganese concentrations where an observable number of pairs would be expected purely on a statistical basis if manganese substitutes for zinc in a random fashion.

The pairs are exchange coupled, probably by superexchange through the sulphurs. The optical absorption spectra of the pairs have been studied by McClure [42]. Brumage *et al* [43] have analysed their contribution to the magnetic susceptibility. The most detailed information has been obtained by Röhrig and Räuber from EPR experiments [44]. A Mn^{2+} has the same $(3d)^5$ configuration as Fe^{3+}. In a pair the two spins 5/2 of the $^6S_{5/2}$ states are coupled to form two-particle states of total spin 0, 1, 2, 3, 4, and 5, the 0 state lying lowest. Röhrig has observed resonances due to the states of total spin 1, 2, and 3. Since these are excited states the intensities of the resonance are strongly temperature dependent, and the energy separations of the states are extracted from the temperature dependence. The spectra are twelvefold and display C_{2v} symmetry with a $\langle 1\,1\,0\rangle$ symmetry axis. There is a prominent hyperfine splitting from the nuclear moments of two equivalent Mn^{2+} nuclei. States 4 and 5 lie at much higher energy and are sparsely populated at the experimental temperatures. The exchange coupling is characterized by an isotropic exchange parameter $J = 35.8\ cm^{-1}$ with much smaller anisotropic components. The coupling is antiferromagnetic, as in βMnS.

5. Conclusion

Association of point defects in a crystal is possible when the temperature of the crystal is small compared with the binding energy of the associate and can be expected to occur if at least one component of the associate is mobile at that temperature. In the II-VI compounds impurities are self-compensated. Associates of impurities with native defects and with other impurities have been observed.

Much information about the microscopic structure of associates characterized by well localized wave functions has been obtained through optical and magnetic resonance experiments. Often the atoms comprising the associate are observed directly by EPR through their nuclear hyperfine splittings. A striking feature of the experimental data is that associates are almost always found with a single small spacing between components. That is, if associates with larger separation exist, they are very few in number compared with those observed. Such "excited" associates would in general be observable if present in sufficient numbers. For example in the Appendix it is shown that a single electronic charge at a distance of about 11 Å from a substitutional Yb^{3+} would produce an easily observable 1 % anisotropy in the Yb^{3+} g factor.

In only a few cases have EPR and optical measurements been correlated to show that the same associate is observed by both methods. More such combined experiments would be useful, especially in the case of copper doping, where both the luminescence and EPR data are complex and at present not well understood.

Almost no experimental information is available about the electrical effects due to the various associates described above. It was possible to obtain such detailed structural information because these defects have deep lying ground levels with respect to the band edge. Therefore, they do not appreciably release thermally carriers at room temperature. However, they may compensate shallow centres. When one dopes a crystal with the intention of providing a desired number of carriers, he usually will find that a portion of the dopants will associate with each other or with native defects. This is the self-compensation effect.

Now that the structures of many associates are known, it would be interesting to monitor associate formation and make comparisons with theoretical predictions. In many cases it is possible to observe by EPR not only the associate but also at least one of the unassociated simple defects which combine to form it. Often more than one charge state of a defect is observable. Concentrations of magnetic defects can be measured with the aid of a reference standard, but this has rarely been done. More careful coordination of optical, EPR, and defect chemical methods should yield much new information on association phenomena.

Acknowledgement

I wish to thank R. Röhrig for sending me the recent results on manganese pairs.

Appendix

Yb^{3+} has the $(4f)^{13}$ configuration. The two multiplets separated by a 10^4 cm^{-1} spin orbit splitting are $^2F_{5/2}$ and the lower lying $^2F_{7/2}$. In tetrahedral symmetry $^2F_{7/2}$ splits into two Kramers doublets Γ_6 and Γ_7 and a quartet Γ_8. In the II-VI compounds the ground state of substitutional Yb^{3+} is Γ_6 with wavefunctions

$$|\Gamma_6 \pm\rangle = (\sqrt{3}/2)\,|M_j = \pm 5/2\rangle - (1/2)\,|\mp 3/2\rangle\,. \quad (4)$$

The isotropic resonance of this state is characterized by $g = 24/7$. Let us estimate the distance R from the Yb^{3+} at which an impurity of one electronic charge $-q$ will produce a 1 % anisotropy in the g factor.

The line joining the Yb^{3+} and the other impurity will be taken to be the z-axis. The potential at position r near the Yb due to the charge $-q$ can be expanded in the (small) parameter r/R. The largest term of importance for the effect of interest is

$$V_2 = (-q/2R^3)(3z^2 - r^2)\,. \quad (5)$$

The corresponding energy is $-qV_2$. For calculations involving only states of the $^2F_{7/2}$ manifold this energy term can be expressed in the operator equivalent form

$$(2/63)\,(q^2\langle r^2\rangle/2R^3)\,O_2^{\circ}\,, \quad (6)$$
$$O_2^{\circ} = 3J_z^2 - 63/4\,.$$

$\langle r^2\rangle$ is the expected value of r^2 for an electron in a 4f orbital of Yb^{3+}. This operator will mix into Γ_6 a part of the Γ_8 state

$$|\Gamma_8 a \pm\rangle = (1/2)\,|\pm 5/2\rangle + (\sqrt{3}/2)\,|\mp 3/2\rangle,$$

and this causes anisotropy in the g factor. The g factors calculated from the perturbed Γ_6 state are

$$g_{\parallel} = 24/7 - (288/7)A/\Delta\,, \quad (7)$$
$$g_{\perp} = -24/7 - (144/7)A/\Delta\,.$$

A is the coefficient of O_2° in Equation 6 and Δ is

the energy separation between Γ_6 and Γ_8. The anisotropy is

$$\| g_\parallel \| - | g_\perp \| = (432/7)A/\Delta \,. \qquad (8)$$

This is 1% of 24/7 if $R = 11$ Å. A reasonable value for the energy separation $\Delta = 500$ cm^{-1} was assumed. The exact value is not so critical since R is proportional to $\Delta^{-1/3}$.

The smallest detectable anisotropy of an EPR line depends upon the linewidth. Even in the case of CdTe, where the linewidth is largest, a 1% anisotropy would be observable.

References

1. C. H. HENRY, K. NASSAU, and J. W. SHIEVER, *Phys. Rev. Letts.* **24** (1970) 820 and references therein.
2. O. F. SHIRMER, *J. Phys. Chem. Solids* **29** (1968) 1407.
3. F. A. KRÖGER, "The Chemistry of Imperfect Crystals" (North-Holland, Amsterdam, 1964) Ch. 9.
4. H. REISS, C. S. FULLER, and F. J. MORIN, *Bell System Tech. J.* **35** (1956) 535 and references therein.
5. J. S. PRENER, *J. Chem. Phys.* **25** (1956) 1294.
6. An example of such a calculation is given by KRÖGER, op. cit., p. 267.
7. G. D. WATKINS in "Radiation Damage in Semiconductors" (Academic Press, New York, 1964) p. 97.
8. G. MANDEL, *Phys. Rev.* **134** (1964) A1073.
9. W. L. ROTH in "Physics and Chemistry of II-VI Compounds," ed. M. Aven and J. S. Prener (Wiley, New York, 1967) Ch. 3.
10. T. KODA and S. SHIONOYA, *Phys. Rev.* **136** (1964) A541.
11. J. D. KINGSLEY and M. AVEN, *ibid* **155** (1967) 235.
12. M. D. STURGE in "Solid State Physics", vol. **20**, ed. F. Seitz, D. Turnbull and H. Ehrenreich (Academic Press, New York, 1967) p. 92.
13. R. K. WATTS, *Phys. Rev.* **2B** (1970) 1239.
14. L. C. KRAVITZ and W. W. PIPER, *ibid* **146** (1966) 322.
15. W. C. HOLTON, R. K. WATTS, and R. D. STINEDURF, *J. Crystal Growth* **6** (1969) 97.
16. J. SCHNEIDER, B. DISCHLER, and A. RÄUBER, *J Phys. Chem. Solids* **29** (1968) 451.
17. W. C. HOLTON, M. DE WIT, T. L. ESTLE, B. DISCHLER, and J. SCHNEIDER, *Phys. Rev.* **169** (1968) 359.
18. R. C. KEMP, *J. Phys. C.* **2** (1969) 1416.
19. *Idem, Phys. Stat. Sol.* **42** (1970) 795.
20. K. MORIGAKI and T. HOSHINA, *J. Phys. Soc. Japan* **23** (1967) 318.
21. W. C. HOLTON, M. DE WIT, and T. L. ESTLE in "International Symposium on Luminescence", ed. N. Riehl and D. Kallmann (Karl Thiemig, Munich, 1966) p. 454 and references therein.
22. R. BOWERS and N. T. MELAMED, *Phys. Rev.* **99** (1955) 1781.
23. P. KASAI and Y. OTOMO, *Phys. Rev. Letts.* **7** (1961) 17.
24. A. RÄUBER, J. SCHNEIDER, and F. MATOSSI, *Z. Naturforschung* **17A** (1962) 654.
25. J. SCHNEIDER, W. C. HOLTON, T. L. ESTLE, and A. RÄUBER, *Phys. Letts.* **5** (1963) 312.
26. J. SCHNEIDER, A. RÄUBER, B. DISCHLER, T. L. ESTLE, and W. C. HOLTON, *J. Chem. Phys.* **42** (1965) 1839.
27. J. SCHNEIDER, B. DISCHLER, and A. RÄUBER, *J. Phys. Chem. Solids* **31** (1970) 337.
28. J. SCHNEIDER in "II-VI Semiconducting Compounds," ed. D. G. Thomas (Benjamin, New York, 1967) p. 40.
29. R. K. WATTS and W. C. HOLTON, unpublished data.
30. J. S. PRENER and D. J. WEIL, *J. Electrochem. Soc.* **106** (1959) 409.
31. K. R. LEA, M. J. M. LEASK, and W. P. WOLF, *J. Phys. Chem. Solids* **23** (1962) 1381.
32. R. K. WATTS and W. C. HOLTON, *Phys. Rev.* **173** (1968) 417.
33. R. S. TITLE and J. W. MAYO, *Bull. Amer. Phys. Soc.* **12** (1967) 41; R. S. TITLE, *ibid* **11** (1966) 14.
34. H. MASUI, *J. Phys. Chem. Solids* **33** (1972) 1129.
35. R. K. WATTS and W. C. HOLTON, *Phys. Rev.* **B2** (1970) 4882.
36. A. F. WELLS, "Structural Inorganic Chemistry" (Oxford University Press, London, 1967) pp. 645 and 657.
37. W. C. HOLTON, M. DE WIT, R. K. WATTS, T. L. ESTLE, and J. SCHNEIDER, *J. Phys. Chem. Solids* **30** (1969) 963.
38. J. DIELEMAN, S. H. DE BRUIN, C. Z. VAN DOORN, and J. HAANSTRA, *Philips Res. Reports* **19** (1964) 311.
39. J. SCHNEIDER and A. RÄUBER, *Solid State Commun.* **5** (1967) 779.
40. S. SHIONOYA, K. URABE, T. KODA, K. ERA, and H. FUJIWARA, *J. Phys. Chem. Solids* **27** (1966) 865.
41. K. URABE, S. SHIONOYA, and A. SUZUKI, *J. Phys. Soc. Japan* **25** (1968) 1611.
42. D. S. MCCLURE, *J. Chem. Phys.* **39** (1963) 2850.
43. W. H. BRUMAGE, C. R. YARGER, and C. C. LIN, *Phys. Rev.* **133** (1964) A765.
44. R. RÖHRIG and A. RÄUBER, to be published. A brief description of results was presented at the 13 April 1972 meeting of the Deutsche Physikalische Gesellschaft in Freudenstadt.

Received 8 January and accepted 14 February 1973.